Short-Range Ultra-Broadband Terahertz Communications: Concepts and Perspectives

Radoslaw Piesiewicz[1,5], Thomas Kleine-Ostmann[2,5], Norman Krumbholz[3,5], Daniel Mittleman[4], Martin Koch[3,5], Joerg Schoebel[3,5], and Thomas Kürner[1,5]

[1]Institut für Nachrichtentechnik, Technische Universität Braunschweig
Schleinitzstr. 22, 38106 Braunschweig, Germany
(R. P.) Tel: +49 531 391 2414; Fax: +49 531 391 5192; E-mail: r.piesiewicz@ieee.org
(T. K.) Tel: +49 531 391 2416; Fax: +49 531 391 5192; E-mail: t.kuerner@tu-bs.de

[2]Physikalisch-Technische Bundesanstalt, AG 2.21 – Elektromagnetische Felder
Bundesallee 100, 38116 Braunschweig, Germany
Tel: +49 531 592 2210; Fax +49 531 592 2256; E-mail: Thomas.Kleine-Ostmann@ptb.de

[3]Institut für Hochfrequenztechnik, Technische Universität Braunschweig
Schleinitzstr. 22, 38106 Braunschweig, Germany
(N. K.) Tel: +49 531 391 2011; Fax: +49 531 391 2045; E-mail: norman.krumbholz@ihf.tu-bs.de
(M. K.) Tel: +49 531 391 2003; Fax: +49 531 391 2045; E-mail: martin.koch@ihf.tu-bs.de
(J. S.) Tel: +49 531 391 2002; Fax: +49 531 391 2045; E-mail: j.schoebel@tu-bs.de

[4]ECE Department, MS 366, Rice University
6100 Main Street, TX 77005 Houston USA
Tel: +1 (713) 348-5452; Fax: +1 (713) 348-5686; E-mail: daniel@rice.edu

[5]Terahertz Communications Lab, Braunschweig, Germany

Abstract

We propose the concept of ultra-broadband terahertz communication, based on directed non-line-of-sight (NLOS) transmissions. Potential applications of such a system supporting multi-gigabit data rates are given, and put into the context of currently emerging WLANs/WPANs. The technology and propagation constraints serve as boundary conditions for the determination of the required antenna gain to support ultra-broadband communication. Resulting high-gain antenna requirements will necessitate highly directed transmissions. We propose the use of omni-directional dielectric mirrors to support directed NLOS paths. Their performance is investigated with ray-tracing simulations of a terahertz propagation channel in a dynamic office environment, which is calibrated with measured building-material and mirror parameters. We demonstrate that a directed NLOS path scheme will make a terahertz communication system robust to shadowing. Furthermore, we show that dielectric mirrors covering only parts of the walls will significantly enhance the signal coverage in a typical indoor scenario.

Keywords: Broadband communication; wireless LAN; terahertz communication; terahertz systems; electromagnetic propagation; communication channels; mirrors; ray tracing

1. Introduction

In recent years there has been an unprecedented growth in the development and deployment of wireless communication systems. The flexibility of wireless communications gives rise to a multitude of potential applications in our society, which is becoming increasingly dependent on information transmission and processing. The interest in short-range wireless communications is accompanied by an increasing need for higher data rates, as numerous new multimedia broad-bandwidth demanding applications proliferate at a great pace.

Extrapolating the rapid growth of wireless data rates that we have seen over the last three decades – where the wireless capacity has been increasing two-fold every 18 months – leads to the unambiguous conclusion that data rates of about 15 Gbps will be needed 10 years from now [1]. Furthermore, data rates in the nomadic traffic will be approaching the capacities of wire-line communication systems.

ISSN 1045-9243/2007/$25 ©2007 IEEE

Gigabit data rates of future wireless communication systems will open the door to a variety of applications demanding ultra-broad bandwidth. Some of these can already be foreseen, and others will undoubtedly emerge as technology progresses. Among the applications that are already foreseen is the wireless extension of the next-generation broadband-access fiber-optic networks. They will support data rates of tens of gigabits, and are expected to replace xDSL [the various types of digital subscriber line] and cable-modem access networks [2]. A similar application can be conceived as a wireless extension of the IEEE 802.3ae standard for high-speed wired local networks, commonly referred to as Gigabit Ethernet, which supports 10 Gbps transmission. Wireless Gigabit Ethernet access, delivered to the desktop, would then facilitate bandwidth-intensive applications like online training, peer-to-peer collaboration, file transfers, and database mining, for example in telemedicine applications. A multi-gigabit communication system could also be operated as a wireless bridge between lower-data-rate WLANs/WPANs (wireless local-area networks/wireless personal-area networks) and access networks, and thus could enhance their interoperability by providing fixed multi-gigabit wireless access. Furthermore, ultra-broadband indoor picocells could be deployed in a given area to respond to the demand for a high aggregate capacity from a number of mobile users, each of whom would be supplied with multimedia-level data rates. A possible corresponding scenario is a scientific conference, where each of the participants can download multimedia data in real time, and concurrently participate in various sessions. Gigabit wireless systems could also find use in supporting wireless virtual-reality applications, for example, computer games. Last but not least, military applications for ultra-high-speed communications in the battlefield can be conceived.

2. The Quest for Bandwidth

Ultra-broadband applications will fall predominantly in the realm of WLANs and WPANs. Hence, they will require the corresponding wireless technologies that will support multi-gigabit data rates. In the following section, we briefly review the current and emerging technologies behind WLANs and WPANs, with emphasis on their ability to support ultra-broadband applications.

2.1 Current and Emerging Wireless Systems

Current WLAN standards comprise IEEE 802.11b,g,a, and offer data rates up to 54 Mbps at 2.4 GHz and 5 GHz. The 83 MHz total bandwidth in the license-free 2.4 GHz ISM band is divided into channels, each of which is 22 MHz wide. For the case of the 5 GHz band, the total bandwidth of 240 MHz in the US and 160 MHz in Europe is split into 20-MHz-wide channels.

The upcoming WLAN IEEE 802.11n standard, which will be an improved version of the 802.11g,a standards, is expected to provide data rates around 100 Mbps in the mandatory modes, and up to 600 Mbps in optional modes [3, 4]. The planned enhancements are based on orthogonal frequency-division multiplexing (OFDM), multiple-input multiple-output (MIMO) techniques, and improved coding. In 2003, the "Wireless Gigabit with Advanced Multimedia" (WIGWAM) project was started in Germany, which aims to deliver data rates up to 1 Gbps [5]. It will be based on OFDM, MIMO, and efficient MAC (medium access control) protocols. It will work in the frequency band of 5 GHz, with extensions to the 17, 24, 38, and 60 GHz bands, with an 802.11 fallback option.

Even though the progress of WLAN technologies is impressive, the data rates of the emerging systems will be limited to 1 Gbps, and will satisfy the demand for only the next few years. However, in the long run, new technology solutions will be needed to support future nomadic multi-gigabit applications.

In case of WPAN technologies, there is currently the Bluetooth standard, with a 1 Mbps data rate provided in the 2.4 GHz ISM band in 79 channels, each of which is 1 MHz wide. Providing an enhanced data rate, the Bluetooth 2 standard will achieve 3 Mbps. Other examples of current WPAN technology are systems where the physical layer is accommodated in the infrared (IR) frequency range. These systems deliver maximum data rates up to several hundred Mbps [6]. However, the poor sensitivity of incoherent receivers, high diffuse-reflection losses, high ambient-light noise, and a limited power budget due to eye-safety limits preclude the realization of higher data rates [7].

The emerging WPAN standards belong to the IEEE 802.15.3 family. In particular, the 802.15.3a task group is developing a standard based upon ultra-wideband (UWB) radio technology for high-speed wireless connectivity. This will accommodate systems in the unlicensed 3.1-10.6 GHz frequency band [8]. The data rates realized reach 500 Mbps [9], while the projected data rates will be limited to around 1.3 Gbps [10]. On the other hand, the millimeter-wave band, around 60 GHz, with unlicensed 5 GHz bandwidth in Europe and 7 GHz bandwidth in the US, is also being considered as a potential host for WPAN systems [11]. The newly formed 802.15.3c task group is developing a millimeter-wave-based physical layer for WPANs in the frequency band between 57 and 64 GHz, with data rates aimed at 2 Gbps.

Similarly to the upcoming WLAN technologies, there is also a lot of progress in the field of WPANs. However, like the WLAN, the emerging WPAN technologies will not be able to accommodate future nomadic applications where the data rates demanded will exceed a few Gbps. Clearly, new technology solutions will be needed to enter into the wireless multi-gigabit area.

3. Radio Systems in the Terahertz Range

Most of the present effort towards higher data rates is aimed at enhancing the spectral efficiency of existing or currently developing microwave and millimeter-wave wireless systems. However, the spectral bandwidth of such systems is limited, and they will not be able to support data rates exceeding a few Gbps. In the long run, there is no alternative but to turn towards higher carrier frequencies. Since it is commonly accepted that such high data rates can not be achieved with IR systems, the terahertz range is a logical choice.

The terahertz range spans the frequencies between 300 GHz and 10 THz. It is unregulated, and offers very large bandwidths, in excess of 10 GHz. It has a potential for very high data rates, exceeding by far a few Gbps. However, the THz range is still technologically immature. It has been used mainly for space and astronomy applications, characterized by cryogenic or low (120 K) operating temperatures for the receivers, and very high implemen-

tation costs. New application areas – found in medicine, the environmental and biological sciences, as well as in security and quality control – have emerged only recently. These drive THz research towards cheaper, room-temperature components, and hence pave the way for wireless communication applications.

In the following two sections, we give an overview of the technology of the sources and detectors, as well as stressing propagation constraints relevant for communication at terahertz frequencies.

3.1 Radio Front-End Technology

Radio-communication transceivers can realize signal reception in direct detection, homodyne, or superheterodyne architectures [12]. The functional units of front ends are local oscillators, mixers, power and low-noise amplifiers, filters, and antennas. For the case of a receiver based on envelope detection, a single detection diode can be used in place of a mixer. The availability and parameters of these devices will eventually determine the emergence and potential success of ultra-broadband wireless communications at terahertz frequencies.

There are two main approaches to generating terahertz radiation [13]. In a bottom-up approach, the operating frequency of electronic devices such as vacuum tubes and solid-state sources is further increased by translation of component solutions and techniques from the millimeter-wave range. As an alternative, optical frequencies can be translated into the terahertz range. In this top-down approach, continuous or pulsed terahertz radiation is generated by laser excitation of semiconductors, and nonlinear crystals or lasers are directly operated at THz frequencies.

For the case of the top-down approach, there are a few potential methods for generating THz continuous-wave radiation. One of these is based on IR-pumped gas lasers with output powers between 1 and 20 mW. However, these devices are bulky and very expensive. They hence pose no long-term solution for communication systems. Another technique for generating terahertz CW radiation is photo-mixing. This is a rather inefficient process, where the output powers do not exceed several tens of microwatts. Hence, photo-mixing is well suited for such applications as THz spectroscopy, but not for communications. Newly developed devices, such as quantum-cascade lasers (QCLs), are promising for efficiently generating CW terahertz radiation. Originally, they were operated at frequencies of many tens of THz, in pulsed modes, and at low temperatures. Currently, their operation tends in the direction of room temperature and CW operation of only a few THz. However, room-temperature CW operation is probably not achievable below 2 THz.

The first demonstration of data transmission at terahertz frequencies was reported in [14], using optoelectronically generated radiation. There, a 75 MHz pulse train of broadband terahertz pulses was amplitude modulated to transmit music. Due to the properties of the applied 2DEG (two-dimensional electron gas) modulator, the channel bandwidth was limited to a few kHz. Even though anticipated improvements might allow for a bandwidth extension to a few MHz, multi-gigabit transmission with this method is impossible.

On the other hand, the latest developments in all-solid-state room-temperature terahertz devices offer encouraging prospects for all-electronic approaches to wireless communication systems at terahertz frequencies. Considerable power in the lower THz range (up to 1 THz) can be generated with Schottky-diode-based multiplier circuits (doublers, triplers, and their combinations) [15, 16], pumped with W-band HEMTs (high-electron-mobility transistor) power amplifiers or Gunn-diode oscillators [17-19]. Diode circuits – manufactured in planar substrateless or membrane technology, and mounted in waveguide blocks – allow for semi-monolithic integration with other devices. They can deliver up to 1 mW of output power at 800 GHz, with bandwidths of the order of 15%. Considerably more power, around 20 mW, can be generated for the lower frequencies at 300 GHz. Thus, reliable THz local oscillators for communication purposes could be potentially realized.

Schottky diodes are also very well suited for mixing and detecting applications. Mixers (balanced, single-diode, and subharmonic), with DSB (double-sideband) conversion losses between 6-12 dB and noise temperatures between 600-1800 K for frequencies between 200-700 GHz, have been reported [20-22]. Hence, THz communication receivers based on heterodyne detection could potentially be fabricated. On the other hand, Schottky diodes alone would also allow for the realization of ultra-broadband receivers implementing envelope detection.

More-complex circuit functions, involving switching and amplification, can be realized with transistors. Recently, there has been a lot of progress in this field, with state-of-the-art transistors reaching cutoff frequencies of around 560 GHz for III-V HEMTs, and 380 GHz for SiGe HBTs (heterojunction bipolar transistors) [23]. The former technology allows for higher-frequency operation, but the latter technology is much cheaper, and is hence more promising for cost-effective solutions in the future.

As the dimensions of the circuits scale down with frequency, the functionality of both sources and detectors at terahertz frequencies depends strongly on the fabrication accuracy of the geometrical details of the components. Conventional waveguide technology is limited by an insufficient precision of the mechanical fabrication (milling). Instead, micromachining, with its reproducible and very accurate control of the dimensions of structures at the 1-100 μm level, is currently the technology of choice for the fabrication of terahertz components [24-26].

A combination of top-down and bottom-up approaches for realizing wireless transmission at sub-terahertz frequencies was reported in [27]. There, 10 Gbps line-of-sight transmission at a 120 GHz carrier frequency was accomplished by using a photonic transmitter and a Schottky-diode-based envelope-detection receiver. Although the link realized was inadequate for nomadic applications and prone to shadowing, it clearly showed the potential of achieving ultra-high data rates, in excess of 10 Gbps, at frequencies approaching the terahertz range. Furthermore, a realization of the transmitter exclusively in all-electronic components would most likely allow decreasing dimensions and reducing costs, making the technology eventually compact and widely accessible.

Mass-market and consumer-electronics applications of THz communication systems require a low-cost, high-volume fabrication technology. Although GaAs or InP technologies may enable millimeter-wave integrated circuits with sufficiently high operation frequency, their potential for scaling to high volume and low cost is rather limited. SiGe BiCMOS technology [28, 29] – which provides high-performance RF processes based on mature CMOS with shared line, tooling, and volumes – has been available for quiet a while. Therefore, RF functions can be integrated with ASIC (appli-

cation-specific integrated circuit)-compliant CMOS technology, which allows for system-on-chip implementations and integration of mixed-signal functions. For more cost-effective solutions with lower performance, RFCMOS consists primarily of an enhancement of digital CMOS with improved RF models and devices.

The status and directions of silicon-based RF technologies were described in detail in [29]. Presupposing that device scaling and performance increases will continue in the same way as we have seen over the last 10 years [28, 29], we extrapolate device performance along the technology nodes defined in the ITRS (International Technology Roadmap for Semiconductors) roadmap [30]. Figure 1 shows the projection of the transit frequency, f_T, as a function of technology node and time. As examples, the HP labels refer to IBM's SiGe BiCMOS technology. The average increase of f_T between two successive generations was determined to be slightly above 1.5. On average, the maximum f_T of SiGe BiCMOS npn HBTs is 2.2 times the f_T of RFCMOS n-channel FETs for the same technology node [29]. The implementation of SiGe BiCMOS lags approximately 1.5 generations behind CMOS [28-30].

Assuming that f_T is a suitable figure of merit, and that a margin factor of two to 10 between operation frequency and peak f_T is required to achieve reasonable circuit performance, a corridor of f_T as a function of application frequency is given in Figure 1, in conjunction with typical applications. As a result, it can be expected that circuits operating near 300 GHz may be realized in about 15 years using 32 nm or 22 nm SiGe BiCMOS technology.

Apart from front-end semiconductor technology, challenging requirements will be placed on signal processing for THz communications to deliver speeds of up to or more than 20 Gbps. However, digital techniques and ICs that are capable of delivering multi-gigabit operational speeds are already a well-established field of research. The circuits that handle 10-40 Gbps signals are already available, and further progress in operating speeds is expected [31]. Also, the ultra-fast ICs that are being developed for fiber-optic communication could be accommodated to feed THz wireless front ends [32].

3.2 Propagation Phenomena

Apart from technological issues, the propagation phenomena will also impose constraints on potential future wireless communication systems at terahertz frequencies. When propagating, electromagnetic waves suffer from spreading of the energy, as well as from clear-air atmospheric and adverse weather conditions [33]. The effect of spreading of the energy, i.e., free-space attenuation, is quantitatively described by the Friis transmission formula. The received power due to the free-space attenuation of the propagating waves is proportional to the square of the wavelength, and inversely proportional to the square of the propagated distance. The free-space attenuation for a 10 m communication link and at frequencies between 300 GHz and 1 THz is between 102 dB and 112 dB.

The influence of the atmosphere and weather on the propagation of radio waves manifests itself in attenuation, phase-shift, and angle-of-arrival variations [34]. The phenomena comprise molecular absorption (mainly due to water vapor and oxygen),

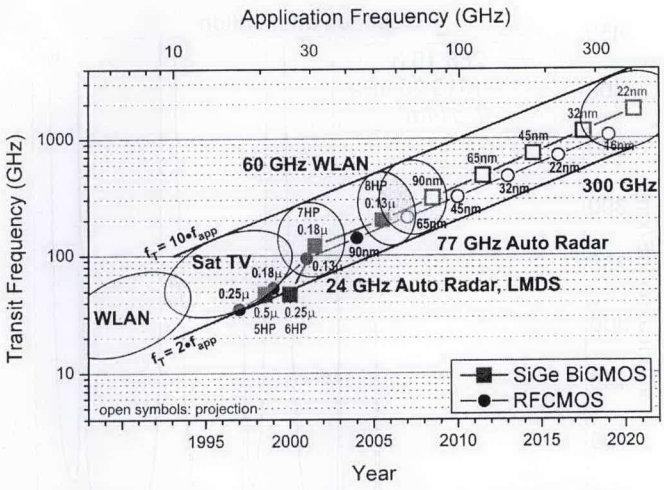

Figure 1. A projection of the transit frequency for SiGe BiCMOS and RFCMOS technologies as a function of the technology node and year. Applications require a margin factor of two to 10 between f_T and the application frequency.

scattering by hydrometeors, and scintillation. In the case of molecular (gaseous) absorption, water vapor is the basic absorbing component in the atmosphere, with very large attenuation values in certain bands above 300 GHz. Oxygen affects radiowave propagation mainly around the frequency of 60 GHz. The attenuation values due to molecular absorption can reach hundreds of dB/km, but there are also a few frequency windows where the attenuation is below or near 60 dB/km. Scattering by hydrometeors is relevant only for outdoor environments, and occurs in rain, fog, and in clouds. In the case of rain, attenuation for the frequencies above around 300 GHz depends only on the rain rate, and can reach values up to 100 dB/km. For the case of propagation through fog and clouds, the attenuation levels depend on the frequency and on the concentration of droplets, and can reach values as high as several tens of dB/km. Scintillation, occurring mainly in outdoor environments, manifests itself in rapid amplitude fluctuations of the propagating signal. This can cause fading of the signal amounting to a few dB.

For indoor and clear-air outdoor applications the free-space path loss and the attenuation due to the molecular content of the atmosphere will be decisive for the operation of future wireless communication systems at terahertz frequencies. These phenomena are illustrated in Figure 2 and Figure 3. Figure 2 depicts the values of gaseous attenuation for a US Standard Atmosphere. Figure 3 depicts the cumulative influence of free-space and gaseous attenuation as functions of both link distance and frequency.

As can be noted from Figure 2, there are five frequency windows located between 300 GHz and 1 THz. The associated center frequencies, corresponding attenuation levels, and bandwidths are listed in Table 1. The bandwidths were calculated as the frequency windows where the attenuation deviated by not more than 30 dB/km from the minimum values occurring at the center frequencies. As the center frequencies increase, the bandwidths and attenuation levels also rise. The maximum attenuation does not exceed 80 dB/km.

Taking into account free-space attenuation, the influence of adverse weather conditions, and absorption levels in the frequency windows, it can be concluded that future ultra-broadband terahertz wireless-communication systems will most likely be limited to

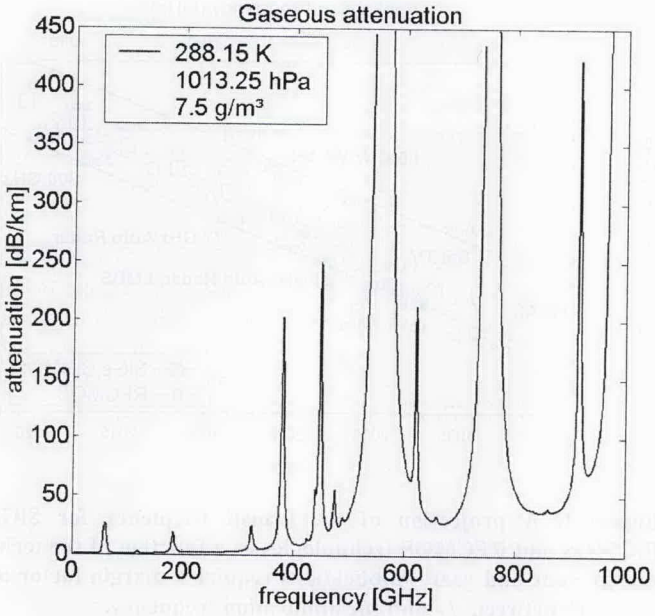

Figure 2. Atmospheric attenuation in the 0-1 THz range.

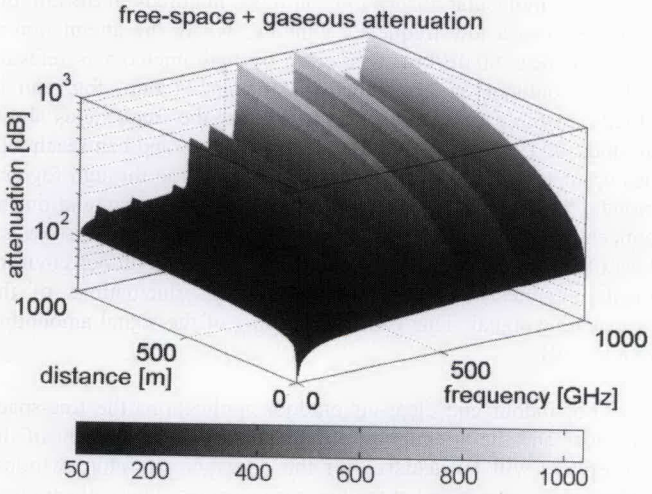

Figure 3. The cumulative free-space and gaseous attenuations in the 0-1 THz range.

Table 1. The parameters of the frequency windows from Figure 2.

Center Frequency [GHz]	Bandwidth [GHz]	Attenuation [dB/km]
300	47	3
350	47	7
410	51	12
670	87	38
850	111	51

medium-link and short-link indoor applications. Outdoor scenarios are conceivable in places where adverse weather conditions are rare.

4. Terahertz Communication

4.1 Choice of the Frequency Window

The carrier frequency of choice for future THz communication systems could be located in one of the frequency windows between 300 GHz and 1 THz. There are already all-electronic room-temperature components, which, after further development and optimization, will most likely be appropriate for ultra-broadband communication purposes. Furthermore, atmospheric attenuation in the windows is still moderate, especially for the prospective medium- and short-link applications. Above 1 THz, atmospheric damping becomes so severe that maintaining a sufficient link budget together with the ultra-broad bandwidth required by the high Gbps data rate would be very difficult.

In the following discussion, the second frequency window, centered at 350 GHz, was chosen. It lies completely in an unregulated region, and offers relatively low values of atmospheric attenuation. Furthermore, the availability of all-electronic components in this frequency range is better, compared to higher-frequency windows.

4.2 Required Antenna Gain

We start with the knowledge of atmospheric and free-space path losses at the frequency of 350 GHz and different distances between transmitter and receiver. The analysis of potential THz front-end components indicated that the system will be power limited (the maximum achievable transmit power will be not more than 0 dBm). Hence, in order to compensate for high propagation losses, it can be expected that high antenna gains will be needed. Thus, with this in mind, we performed link-budget analyses to calculate the required antenna gains for different link distances and signal bandwidths.

A representative receiver front-end architecture was assumed for the carrier frequency, f_c, of 350 GHz. The front end, shown in Figure 4, was composed of an antenna with a waveguide transition, a down-converting mixer integrated with a local oscillator, and an IF amplifier. As would be conventionally expected, a low-noise amplifier was missing before the first down-converting stage. This was due to the present lack of amplifier technology at such high frequencies. However, this may change in the future, with the progress of terahertz technology.

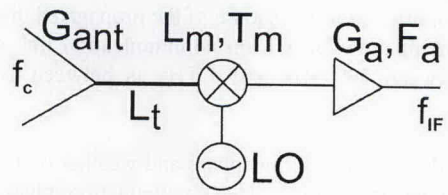

Figure 4. The representative receiver front-end architecture assumed for link-budget analysis.

Table 2. The circuit parameters for the front-end components from Figure 4.

L_t	0.5 dB
L_m	6.5 dB
T_m	800 K
G_a	24 dB
F_a	3.5 dB

L_t stands for the loss factor of the waveguide transition connecting the antenna to the mixer. L_m and T_m represent the conversion loss and DSB (double sideband) noise temperature of the down-converting mixer, respectively. The values of the parameters of the mixer, which was manufactured in traditional E-plane split-block waveguide technology, were taken according to [35]. It was assumed that the local oscillator delivered enough power to drive the mixer. G_a and F_a are the gain and noise figure of the IF amplifier, respectively. The intermediate frequency, f_{IF}, was chosen to be 50 GHz. This was high enough to accommodate the large modulation bandwidths that will be needed to provide multi-gigabit data rates. The technology for amplifiers in this frequency range is well established. Since we considered potential indoor wireless systems, the physical temperature of the receiver antenna and of the waveguide transition were assumed to be $T_0 = 290$ K. Also, the antenna pointed at the background with a room temperature of $T_0 = 290$ K. The values assumed for the circuit parameters in Figure 4 are listed in Table 2.

A first-stage down-converting mixer will be an essential part of a terahertz receiver front end. Its design and parameters will determine the performance of the receiver. Its integration with an antenna and with a first amplifying stage will reduce manufacturing costs, and hence will eventually make terahertz technology cost effective for communication applications.

For the receiver front end at hand, but without the antenna, a noise analysis was performed according to [12]. The overall noise figure, F_{tot}, and the overall gain, G_{tot}, were calculated. F_{tot} amounted to 10.2 dB, while G_{tot} equaled 17 dB. The application of integration techniques should allow for the reduction of the overall noise figure of a terahertz receiver front end in future practical realizations.

The absolute value of the overall noise figure, F_{tot}, was converted into the overall noise temperature, T_{tot}:

$$T_{tot} = (F_{tot} - 1)T_0. \tag{1}$$

The resulting overall noise temperature was $T_{tot} = 2733$ K.

In the next step, we calculated the output noise power, N_{out}, of the receiver. This is the noise power that is relevant for the demodulation process. For this, the specification of the signal bandwidth, B, was needed. We varied the bandwidth of the modulating signal between 5 and 50 GHz, which corresponds to the available bandwidth of the frequency window at 350 GHz. The output noise power, N_{out}, is given as

$$N_{out} = 10\log\left[k(T_0 + T_{tot})B\right] + G_{tot}, \tag{2}$$

where k stands for Boltzmann's constant. The temperature, T_0, in Equation (2) corresponds to the influence of the receiver antenna.

Additional system parameters were considered in the next step of the link analysis. They were the needed modulation margin, M_m, and the system margin, M_s. The system parameters and their assumed values are listed in Table 3.

The system margin, M_s, consists of the fade margin (5 dB) and the system reserve (5 dB). The fade margin accounts for the fading of the signal due to potential antenna misalignments and signal scintillation. The system reserve covers all unaccounted losses that might possibly occur in the communication system. The modulation-dependent margin, M_m, designates the value of the signal-to-noise ratio at the output of the front end (SNR_{out}), i.e., at the input to the demodulator. In order to be more precise, it was assumed that the demodulation was based on the BPSK scheme, with a bit-error rate (BER) of 10^{-6}. The choice of BPSK modulation was arbitrary. By changing the value of the modulation-margin parameter, other modulation schemes could be accounted for in the link-budget estimation.

In order to demodulate the information-bearing signal with the given BER, the value of SNR_{out} must be equal to the given modulation margin level, M_m. For the assumed circuit and system parameters, this was guaranteed if the input signal power to the receiver, S_{in}, was

$$S_{in} = M_m + M_s + N_{out} - G_{tot}. \tag{3}$$

For the bandwidth at hand (5-50 GHz), the required input signal power, S_{in}, was calculated to be between –56 and –46 dBm.

In the last step of the link analysis, the power that arrives at the receiver was calculated. The output power from the transmitter was assumed to be 1 mW. The transmitted signal undergoes free-space and atmospheric attenuation. Both of these attenuation mechanisms are distance dependent. We performed calculations for four link distances: 1 m, 3 m, 5 m, and 10 m. For example, for a 10 m link and the chosen center frequency of 350 GHz, the free-space attenuation was 103.3 dB, while the atmospheric attenuation was 0.07 dB. Hence, the total signal attenuation amounted to around 103.4 dB. For a 1 mW transmitter output, the received signal power was then –103.4 dBm. By comparison with S_{in}, the received signal level was too low to successfully demodulate the information-bearing signal. Hence, appropriate measures had to be taken to compensate for the high signal attenuation. However, the available transmitter power levels are limited at such high frequencies. Thus, using high-gain antennas seems to be a reasonable option in order to compensate for the high signal attenuation.

The required antenna gain was calculated as the difference between the estimated sensitivity of the receiver, S_{in}, and the effectively received power due to attenuation for a given transmitter output. Finally, the resulting required antenna gain was halved

Table 3. The system parameters for a link budget analysis.

System margin (M_s)	10 dB
Modulation margin (M_m)	10.5 dB

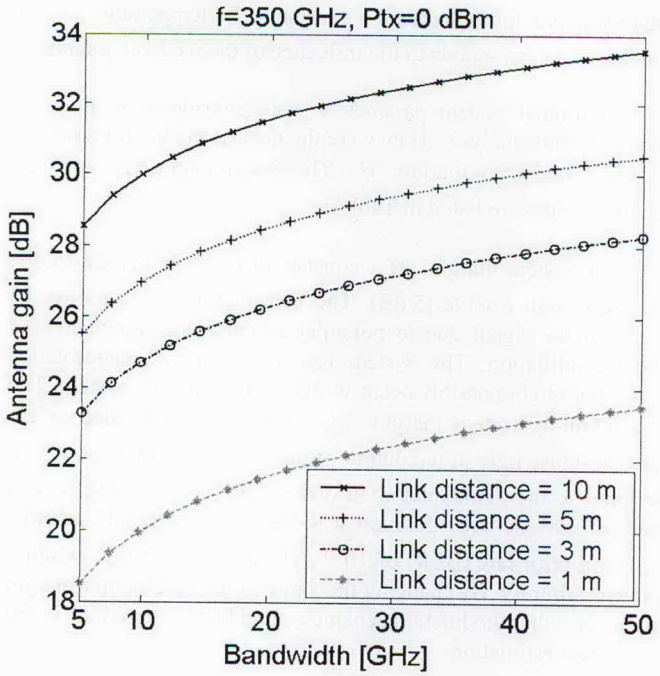

Figure 5. The required antenna gain for a receiver and a transmitter to support high-data-rate communication at 350 GHz for different link distances.

between the transmitter and receiver. This is shown in Figure 5 as a function of signal bandwidth for four different link distances: 1 m, 3 m, 5 m, and 10 m.

It can be seen from Figure 5 that terahertz communication systems will require high-gain antennas. In the case of a 10 m link, an antenna gain between 28 and 34 dB will be necessary. The use of high-gain antennas poses a question about the safety issues with respect to human exposure to the radiation. The maximum power density for general public exposure to time-varying electromagnetic fields is set to 1 mW/cm^2 for frequencies between 2 GHz and 300 GHz [36]. Since there is not yet any regulation pertaining to the THz range, this limit was assumed. The safety clearance for 1 mW output power and 32 dB antenna gain was then 11 cm. This seems to be a reasonable distance with respect to the foreseen applications. The use of lower antenna gains for shorter links will result in even shorter safety clearances.

THz communication systems will rely on directed transmissions with high-gain antennas. This is an important conceptual difference from present-day wireless communication systems, which are based on quasi-omni-directional antennas and non-directed transmissions. The high-directivity requirement implies that a transmitter will have to physically see a receiver, and that communication will predominantly take place over line-of-sight (LOS) links. Also, the higher the antenna gain needed, the smaller is the coverage area, and the more difficult it is to align a receiver with a transmitter. Even if the noise figure of a future more-advanced terahertz receiver is reduced, high-gain antennas will still be needed.

4.3 Indirect Transmission Paths

However, the line-of-sight requirement also brings obvious problems that have to be dealt with: the link can be broken by moving people or other objects that block the direct line-of-sight path. This problem could be solved by alternate transmission routes, supported by directed non-line-of-sight (NLOS) paths that involve reflections off the walls. If a THz communication system could rely on such NLOS "billiard" channels as a backup, a reliable high-bandwidth link could be maintained.

Any viable communication would then take place with antennas looking directly at each other either (LOS case), or indirectly through reflections in the specular direction. The objective of an antenna system will be to dynamically choose the best possible single path, either LOS or NLOS. The requirement that future THz communication systems will have to rely on high-gain antennas, aligned for maximum radiation, has a direct impact on the propagation paths that have to be considered in propagation modeling. In [37], it was shown with simulations and verified with measurements that when working with directive antennas in indoor environments, multipath can be neglected. This comes from the fact that any multipath coming from outside of the maximum-gain direction of the antenna will be attenuated by the antenna radiation pattern. Similar conditions will apply to THz communication systems. Hence, in the further discussion, we neglect multipath effects and treat only single paths, either direct LOS or through directed NLOS specular reflections.

However, reflections off the surfaces of building materials mean that an additional loss term will be added to the propagation losses. Measurements of an amplitude reflection coefficient, Γ, for specular reflections at terahertz frequencies for different common building materials at different incidence angles were reported in [38]. However, a figure of merit that is more useful for link-budget calculations for NLOS paths is the reflection loss, *RL*. Its relationship to the reflection coefficient is as follows:

$$RL = -20\log|\Gamma|. \tag{4}$$

In Figure 6, *RL* coefficients, derived from the reflection coefficients reported in [38], are shown for a frequency of

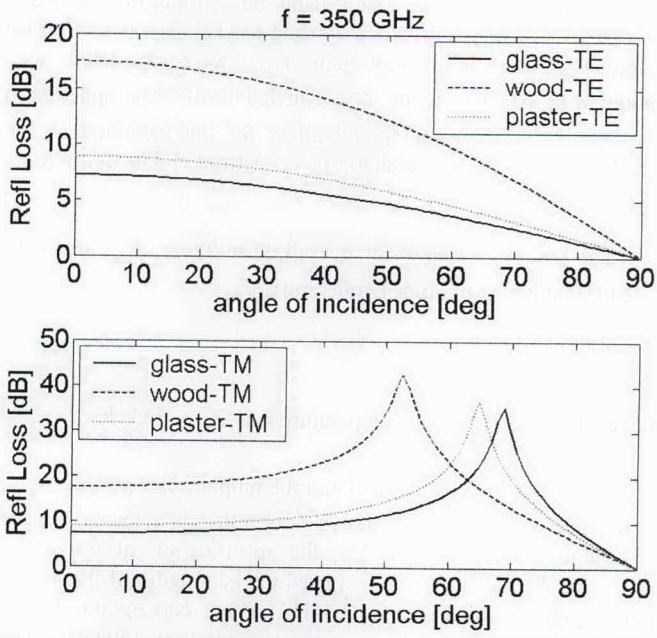

Figure 6. The reflection loss for common building materials for a frequency of 350 GHz as a function of the angle of incidence. From top to bottom, the two plots show the TE and TM polarization cases.

Table 4. The mean values of the reflection loss coefficients in dB.

	TE	TM
Glass	4.6	11.1
Wood	11.7	18.4
Plaster	5.7	12.5

350 GHz. TE and TM polarizations are shown as a function of the angle of incidence for samples of glass, pine wood, and plaster. As expected, the *RL* coefficient is angle dependent, and has higher values for the TM polarization than for the TE polarization for a chosen material. It is a decreasing function of frequency for the TE polarization. In case of the TM polarization, it increases as the angle approaches the Brewster angle, and then decreases as the angle moves away from the Brewster angle. Mean values of the *RL* coefficient for the TE and TM polarizations for the measured materials are listed in Table 4. The maximum values of *RL* can reach 7.2, 17.5, and 8.9 dB for the TE polarization for glass, wood, and plaster, respectively. In the case of the TM polarization, the maximum values of *RL* amount to 35.1, 42.5 and 36.7 dB for the respective materials.

Therefore, in case of NLOS paths, a considerable loss term will be incurred in addition to free-space propagation losses by employing reflections from objects. This loss term will have to be compensated for by increased antenna gain. As a result, the coverage area will be further reduced, alignment issues will be worsened, and planning of the structure of the access cells will become more difficult.

4.4 Dielectric Mirrors

The problem of high reflection losses can be solved by enhancing the reflectivity of building materials. This task can be realized by covering indoor surfaces with THz dielectric mirrors, which have recently been demonstrated [39, 40]. A dielectric THz mirror consists of a stack of pairs of different dielectric materials. Such mirrors are cheap to produce, and can be designed to have excellent reflecting properties. For applications in directed NLOS communication scenarios, a dielectric mirror should have good reflective properties over a broad range of incidence angles. Such a mirror is called omnidirectional, and can be obtained by a proper choice of its refractive indices [41]. A first omnidirectional mirror for the terahertz range was demonstrated in [42]. The structure consisted of five 150 μm thick layers of polypropylene, with a refractive index of 1.53, and four 63 μm thick layers of high-resistivity silicon, with a refractive index of 3.418. The measured and simulated power reflection coefficients of the mirror are shown in Figures 7-10 for incidence angles of 0° and 20°, 40°, 60°, and 89°, respectively. In each of the figures, the results for both TE and TM polarization are depicted.

For the frequencies between 319 and 375 GHz, the power reflection coefficient of the mirror was at least 0.95. The corresponding reflection loss coefficient was less than 0.2 dB. Moreover, the high-reflectivity spectrum of the mirror coincided with the bandwidth of the frequency window centered at 350 GHz. Furthermore, the high-reflectivity property was maintained for all incidence angles and for both TE and TM polarization. These highly reflecting omni-directional mirrors can be used as wallpaper in future terahertz communication systems to support directed

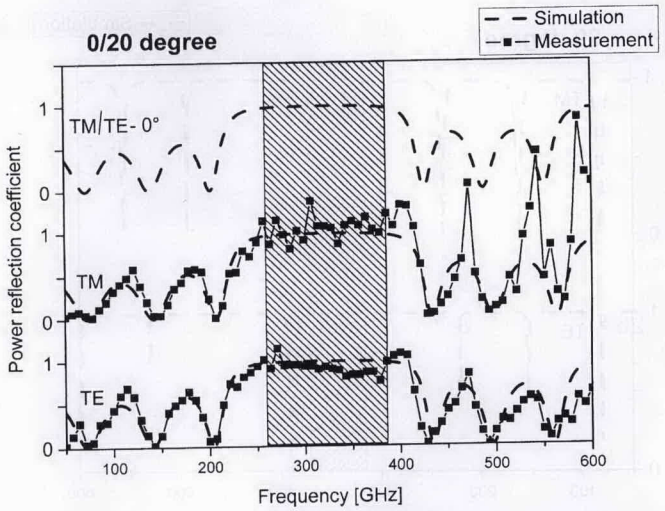

Figure 7. The measured and simulated power reflection coefficient of the mirror structure for angles of incidence of 0° and 20°, and TM and TE polarization.

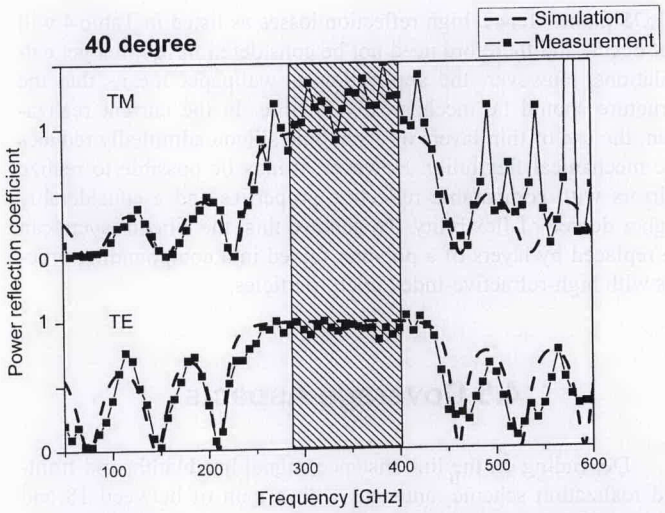

Figure 8. The measured and simulated power reflection coefficient for 40° incidence.

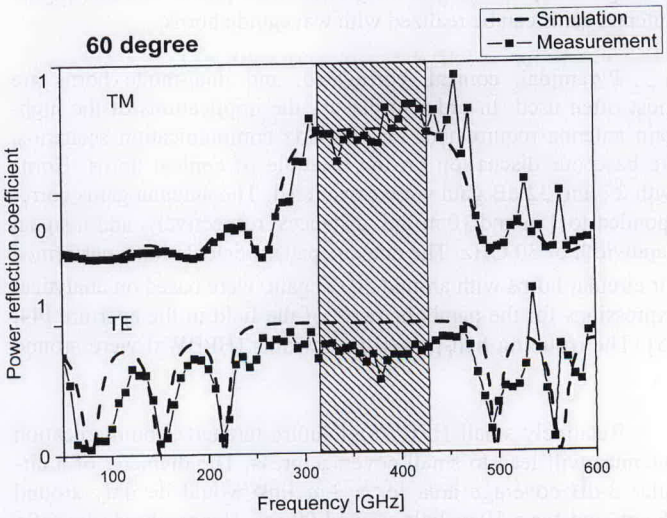

Figure 9. The measured and simulated power reflection coefficient for 60° incidence.

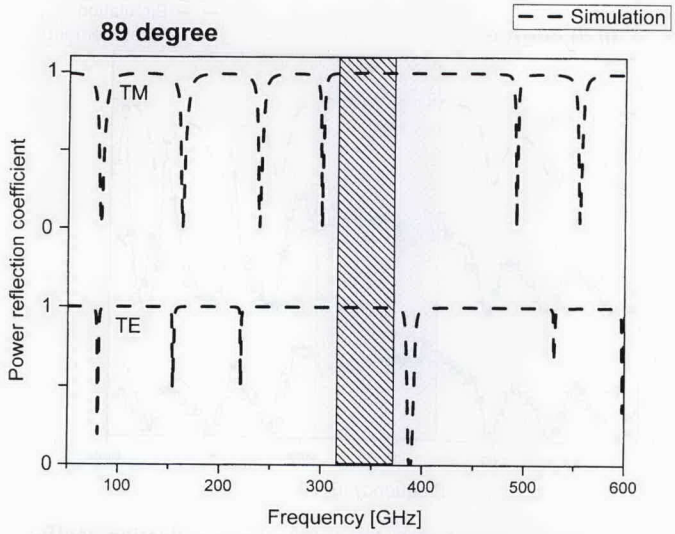

Figure 10. The simulated power reflection coefficient for 89° incidence.

NLOS paths. Hence, high reflection losses as listed in Table 4 will not occur, and therefore need not be considered in link-budget calculations. However, the application as wallpaper means that the structure should be mechanically flexible. In the current realization, the use of thin layers of crystalline silicon admittedly reduces the mechanical flexibility. However, it may be possible to realize mirrors with comparable reflective properties and a considerably higher degree of flexibility. To achieve this, the silicon layers can be replaced by layers of a polymer mixed in a compounding process with high-refractive-index micro-particles.

4.5 Coverage Aspects

Depending on the link distance, signal bandwidth, and front-end realization scheme, antennas with a gain of between 18 and 34 dB will be needed in future terahertz communication systems. Several antenna types have been employed at THz frequencies, including planar antenna structures on dielectric lenses and waveguide horn antennas [43]. While planar antenna structures offer greater potential for integration with planar circuits, higher antenna gains can be realized with waveguide horns.

Pyramidal, conical, corrugated, and dual-mode horns are most often used. In order to discuss the implications of the high-gain antenna requirement for terahertz communication scenarios, we base our discussion on the example of conical horns. Horns with 27 and 32 dB gain were considered. The antenna gains corresponded to 3 m and 10 m link distances, respectively, and a signal bandwidth of 30 GHz. The antenna pattern calculations, performed for circular horns with around 30 dB gain, were based on analytical expressions for the parabolic taper of the field in the aperture [44, 45]. The resulting half-power beamwidths (HPBWs) were around 5°.

Relatively small HPBWs of future terahertz communication antennas will lead to small coverage areas. The diameter of a circular 3-dB coverage area for a 3 m link would be only around 45 cm, and for a 10 m link, around 90 cm. Hence, the design of a tracking system that will allow for signal recovery when the LOS beam is blocked, e.g., due to shadowing or displacement of a receiver, will be rather demanding. Furthermore, in the case of larger rooms – such as, for instance, convention centers – there may be a need for more than one coverage cell. The division of such an area into cells will then represent a major task, and cell-planning issues will emerge. Moreover, the design of an appropriate antenna-switching scheme for NLOS paths will require a thorough investigation.

Altogether, some sort of a multibeam antenna or a phased-array antenna scheme allowing for beam steering will definitely be needed. Presently, there is a lot of research activity on steerable antennas for frequencies from 1 to 77 GHz. Smart antennas for THz frequencies have not yet been demonstrated.

5. Application Scenarios

Future terahertz communication systems will have to rely on directed transmissions with high-gain antennas. Preferably, this will be in the LOS mode, but system robustness (that is, a high degree of immunity to shadowing) will be achieved only if the system can rely on the NLOS mode as a backup. Only if the desired LOS mode cannot be operated, e.g., due to shadowing, will the antenna system then have to choose an optimum directed NLOS path. Both of the communication modes are illustrated in Figure 11.

5.1 Ray Tracing

The performance of both communication modes is demonstrated by an example of a simulated scenario in a furnished room with people inside it. The simulations are based on ray tracing, implemented with the image method [46]. Ray tracing is a deterministic tool for investigating properties of wireless communication channels. Both temporal and spatial channel characteristics can be obtained with it [47]. In the following sections the results of ray-tracing simulations are shown, to underline the presented concept for terahertz communications based on directed NLOS paths.

Wideband measurement results of reflection coefficients for common indoor materials [38] were used to calibrate the ray-tracing calculations. Reflection coefficients of the measured omnidirectional dielectric mirror were also implemented in the simulation environment. The gain of the conical-horn antenna introduced for the 10 m link was considered. It was assumed that an antenna tracking system for NLOS paths was implemented. The ray-tracing calculations took into account specular reflections off the objects, and transmission through the objects. No accounting was made for diffraction and scattering phenomena.

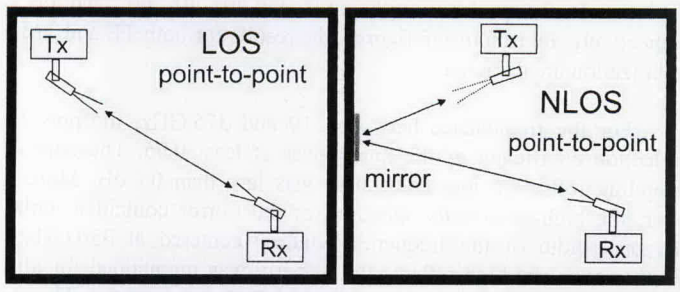

Figure 11. LOS and NLOS transmission modes for future terahertz communication systems.

5.2 Simulated Scenario

The simulated room is shown in Figure 12. It was arranged with furniture. Windows, positioned on the front wall, consisted of metal panels and glass panes. Other objects, such as tables, closets, and book shelves, were made partially of metal and partially of wood. The room had dimensions of 6 m × 5 m × 2.5 m. The walls of this room were covered with plaster.

The transmitter, with an output power of 0 dBm and a frequency of 350 GHz, was placed in the middle of the room, i.e., at $x = 3\,\text{m}$ and $y = 2.5\,\text{m}$, just below the ceiling at a height of 2.3 m ($z = 2.3\,\text{m}$). The position of the receiver was varied on a 15 × 13 grid in the plane $z = 0.95\,\text{m}$ above the floor. The number of points sampled in the xy plane corresponded to the calculated coverage area of a 10 m link. The number of points in the grid was calculated as the rounded ratio of the respective room dimension and the coverage radius.

The presence of people provided a dynamic factor in the simulations, and allowed for the investigation of shadowing. Four persons, modeled as perfectly attenuating surfaces as depicted in Figure 12, were distributed randomly in the room. For each position of the receiver in the grid, ray-tracing simulations were performed for a set of fifty different realizations of the distribution of the persons in the room. On one hand, this number of simulations allowed taking shadowing into account. On the other hand, it kept the numerical complexity within acceptable limits.

5.3 Simulation Results

The simulations were grouped into three distinct parts. The first part showed the performance of directed NLOS paths used to support a shadowing-free communication environment. In the second part, the required area and positions of the mirrors were discussed. In the third part, the performance of the mirrors was investigated with respect to delivered power levels in an enhanced-reflectivity environment.

5.3.1 Shadowing-Free Transmissions

The signal-coverage calculations in the plane of the receiver were performed for LOS, and once-reflected and twice-reflected NLOS paths. The dielectric mirrors were used as wallpaper, and were also placed on the ceiling. The susceptibility of LOS paths and the robustness of the NLOS paths with respect to shadowing are illustrated in Figure 13.

In Figure 13, the worst-case received signal power just above the level of the tables at a height of 1 m above the floor is plotted. Dark areas represent regions where the transmission was blocked. Upon blockage of the transmission, the received signal level was taken to be just below the calculated lowest sensitivity level of −56 dBm. As can be seen, a terahertz link cannot rely on LOS paths only, as there is always the chance that it will be blocked by a person stepping into the beam path. The bright area in the middle of the room for the LOS case was due to the arrangement of the three tables. On the other hand, a few dark areas by once- and twice-reflected NLOS paths near the walls corresponded to the positions of the furniture. Otherwise, transmissions with reflec-

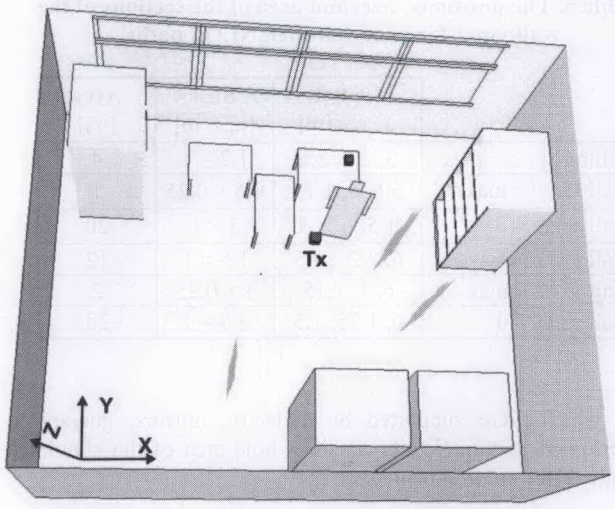

Figure 12. A view of the simulated scenario in an arranged room with people.

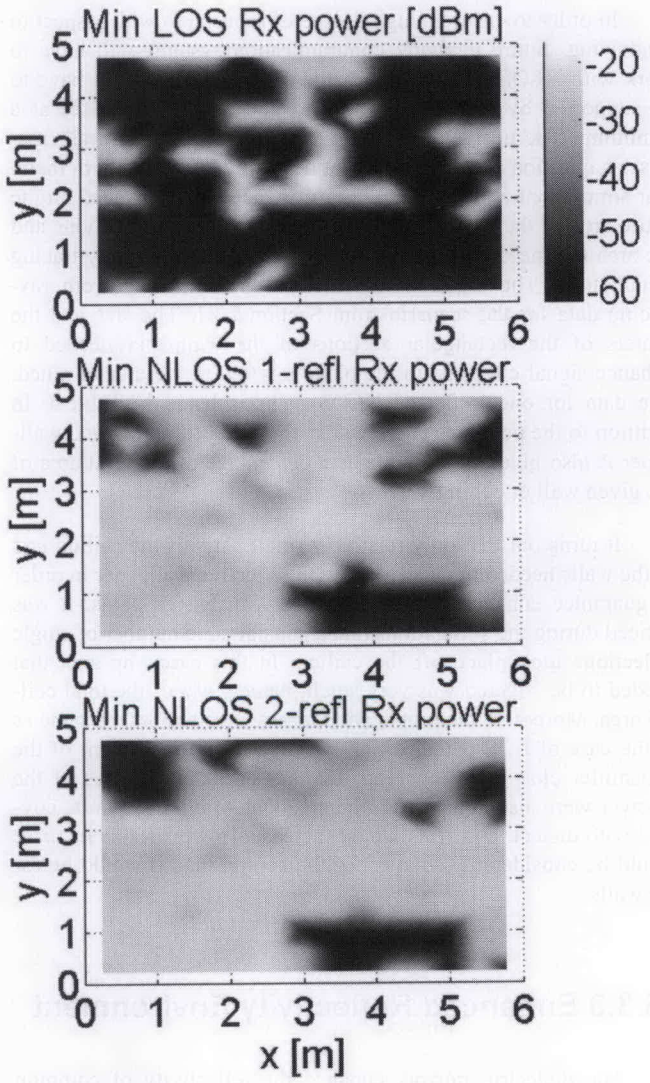

Figure 13. The worst-case received power level (in dBm) 1 m above the floor in a 5 m × 6 m room with typical office furniture and moving people. From top to bottom, the three plots show the power levels resulting from LOS, once-reflected NLOS, and twice-reflected NLOS paths.

Table 5. The positions, size, and area of the sections of the wallpaper for once-reflected NLOS paths.

	Center x, y, z [m]	Size [m × m]	Area [%]
Ceiling xy, $z = \max$	3, 2.5, 2.5	1.2 × 1	4
Wall xz, $y = \max$	5.6, 5, 1.15	0.6 × 0.25	1
Wall xz, $y = 0$	1.5, 0, 1.5	3 × 1	20
Wall yz, $x = \max$	6, 2.25, 1.5	1.5 × 1	12
Wall yz, $x = \max$	6, 1, 1.15	1 × 0.25	2
Wall yz, $x = 0$	0, 1.75, 1.5	3.5 × 1	28

tions, which were supported by dielectric mirrors, guaranteed uninterrupted communication in the whole area of the simulated dynamic office environment.

5.3.2 Area and Positions of Mirrors

In order to ensure a high degree of robustness with respect to shadowing, future terahertz communication systems will have to work with NLOS transmission paths. The reflections will have to be supported by dielectric mirrors to keep reflection losses at a minimum. The necessity for using dielectric mirrors as wallpaper raises a question about the area that needs to be covered with them. Our simulations showed that the mirrors need not be placed on the entire area of the walls and of the ceiling. The exact positions and the area that needs to be covered can be obtained with ray-tracing calculations. The required information was extracted from ray-tracing data for the scenario from Section 5.3.1. The size and the centers of the rectangular sections of the wallpaper needed to enhance signal coverage in the plane $z = 0.95$ m were determined. The data for once-reflected NLOS paths is listed in Table 5. In addition to the positions and the size, the area of the required wallpaper is also given in the table as a percentage of the total area of the given wall or ceiling.

It turns out that only relatively small parts of the ceiling and of the walls needed to be covered with reflective wallpaper in order to guarantee enhanced signal coverage with NLOS paths. It was noticed during the simulations that a considerable number of single reflections took place off the ceiling. In this case, the area that needed to be covered was very small, namely 4% of the total ceiling area. Moreover, the propagation losses were almost the same as in the case of LOS paths, which was due to the placement of the transmitter close to the ceiling. If other horizontal planes of the receiver were also considered, the area that would need to be covered with dielectric mirrors would increase. However, this increase would be considerably smaller for the ceiling than it would be for the walls.

5.3.3 Enhanced Reflectivity Environment

The dielectric mirrors enhance the reflectivity of common building materials. Their application will allow the saving of a few dB in the system margin in the link budget, which would otherwise be needed to compensate for the reflection losses. Hence, the antenna gain can be smaller than otherwise required, and the terahertz communication system will not have to cope with even smaller HPBWs and smaller coverage areas. To illustrate this, the channel was simulated for the case when the dielectric mirrors were used as wallpaper and for the case where the walls were covered only with plaster. In the case of enhanced reflectivity, the mirrors were put at the positions specified in Table 5. The ray-tracing simulations were performed for once-reflected paths in the furnished room, without the presence of people. The distribution of the received power level in the plane $z = 0.95$ m is shown for the cases with and without mirrors in Figure 14 for TM polarization, and in Figure 15 for TE polarization.

When the walls were covered with dielectric mirrors, the received power levels varied between −59 and −21 dBm for both TM and TE polarizations. The mean value of the received power equaled −28 dBm. In the case of plaster walls, the received power level varied between −59 and −27.5 dBm for TM-polarized and between −59 and −26.7 dBm for TE-polarized waves. The mean values were −37.5 dBm and −34 dBm for the TM and TE polarizations, respectively. Hence, the application of dielectric mirrors in typical office environments provided for higher received power levels of 9.5 dB and 6 dB, on average, for TM and TE polarizations, respectively. Furthermore, the signal coverage when using dielectric mirrors was the same for both linear polarization types.

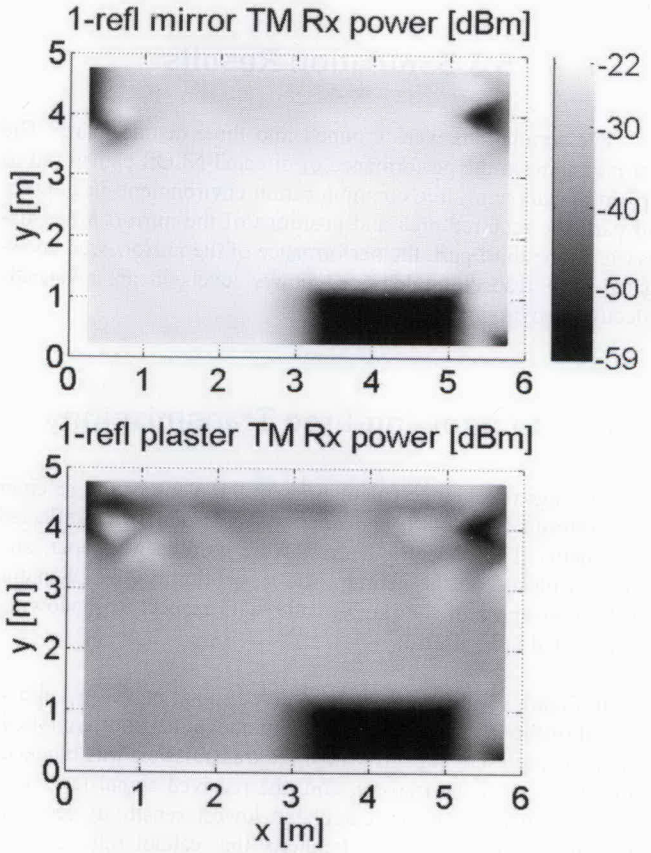

Figure 14. The received power level (in dBm) 1 m above the floor in a 5 m × 6 m room with typical office furniture. From top to bottom, the two plots show the power levels for TM polarization resulting from once-reflected NLOS paths in the room, with and without mirrors.

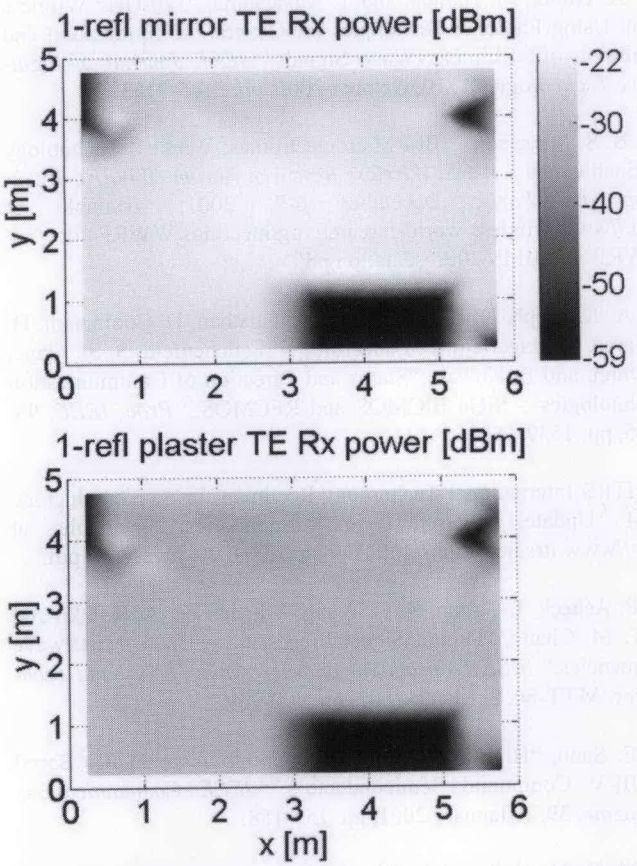

Figure 15. The received power level (in dBm) 1 m above the floor in a 5 m × 6 m room with typical office furniture. From top to bottom, the two plots show the power levels for TE polarization resulting from once-reflected NLOS paths in the room, with and without mirrors.

6. Conclusions

Multi-gigabit-data-rate indoor communication applications, requiring ultra-broad-bandwidth for their operation, are bound to emerge in the future. However, the current and upcoming WLAN/WPAN communication systems will not support data rates in excess of 2 Gbps. New technology, possibly in the terahertz range, is needed. This paper has discussed the technological and propagation conditions for future communication systems that will be accommodated between 300 GHz and 1 THz. The required antenna gain was estimated for varied bandwidths, and link distances for a system with a front-end architecture were set out for operation at 350 GHz. The implications of a resulting high-gain antenna requirement were discussed for prospective communication scenarios, and a concept of indirect transmission paths was proposed. The application of omnidirectional dielectric mirrors to support directed NLOS transmissions was shown.. The performance of such mirrors was investigated with ray-tracing simulations in a dynamic environment of a typical office room, supplemented with material measurements. Directed NLOS transmissions, supported with dielectric mirrors, will make future terahertz communication systems more robust with respect to shadowing. Furthermore, the application of the mirrors will lead to a reduction of the required antenna gain in NLOS scenarios. Hence, the mirrors will contribute to a more effective planning of the coverage area.

7. Acknowledgement

We acknowledge fruitful discussions with Ibraheem A. Ibraheem from the Institut für Hochfrequenztechnik and Axel Junge from the Institut für Elektromagnetische Verträglichkeit, both at the Technical University Braunschweig; and Andreas Czylwik from the Institut für Nachrichtentechnische Systeme at the Technical University Duisburg-Essen.

8. References

1. S. Cherry, "Edholm's Law of Bandwidth," *IEEE Spectrum*, **41**, 7, July 2004, p. 50.

2. S. Zeadally and L. Zhang, "Enabling Gigabit Network Access to End Users," *Proc. of the IEEE*, **92**, 2, February 2004, pp. 340-353.

3. WWiSE IEEE 802.11n Proposal, IEEE 802.11-05/0150r1, March 2005.

4. TgnSync IEEE 802.11n Proposal, IEEE 802.11-04/888r11, March 2005.

5. G. Fettweis and R. Irmer, "WIGWAM, Wireless Gigabit with Advanced Multimedia Support," *Wireless Broadband Forum,* Cambridge, UK, November 2004.

6. D. C. O'Brien, et al., "High-Speed Integrated Transceivers for Optical Wireless," *IEEE Communications Magazine*, **41**, 3, March 2003, pp. 58-62.

7. M. Wolf and D. Kress, "Short-Range Wireless Infrared Transmission: The Link Budget Compared to RF," *IEEE Wireless Communications*, **10**, 2, April 2003, pp. 8-14.

8. S. Roy, J. R. Foerster, V. S. Somayazulu, and D. G. Leeper, "Ultrawideband Radio Design: The Promise of High-Speed, Short-Range Wireless Connectivity," *Proc. of the IEEE*, **92**, 2, February 2004, pp. 295-311.

9. G. R. Aiello and G. D. Rogerson, "Ultra-Wideband Wireless Systems," *IEEE Microwave Magazine*, **4**, 2, June 2003, pp. 36-47.

10. PHY Proposal to IEEE 802.15.3a, IEEE 802.15-03/105r1, March 2003.

11. P. Smulders, "Exploiting the 60 GHz Band for Local Wireless Multimedia Access: Prospects and Future Directions," *IEEE Communications Magazine*, **40**, 1, January 2002, pp. 140-147.

12. D. M. Pozar, *Microwave Engineering, Third Edition*, New York, John Wiley & Sons Ltd., 2005.

13. P. H. Siegel, "Terahertz Technology," *IEEE Transactions on Microwave Theory and Techniques*, **MTT-50**, 3, March 2002, pp. 910-928.

14. T. Kleine-Ostmann, K. Pierz, G. Hein, P. Dawson, and M. Koch, "Audio Signal Transmission over THz Communication Channel Using Semiconductor Modulator," *Electronics Letters*, **40**, 2, January 2004, pp. 124-126.

15. J. Ward, E. Schlecht, G. Chattopadhyay, A. Maestrini, J. Gill, F. Maiwald, H. Javadi, and I. Mehdi, "Capability of THz Sources Based on Schottky Diode Frequency Multiplier Chains," *IEEE MTT-S Digest*, 2004, pp. 1587-1590.

16. T. W. Crowe, W. L. Bishop, D. W. Porterfield, and J. L. Hesler, "Integrated Terahertz Sources and Receivers," *Proceedings IEEE 29th International Conference on Infrared and Millimeter Waves and 12th International Conference on Terahertz Electronics*, September 2004, pp. 85-86.

17. H. Zirath, J. Grahn, N. Rorsman, A. Mellberg, J. Stake, I. Angelov, and P. Starski, "InP HEMTs and HBVs for Low Noise and Ultra-High Speed: Device and Circuit Research at Chalmers University of Technology," *Proc. Intl. GAAS Symp.*, 2003, pp. 469-472.

18. H. Eisele and R. Kamoua, "Submillimeter-Wave InP Gunn Devices," *IEEE Transactions on Microwave Theory and Techniques*, **MTT-52**, 10, October 2004, pp. 2371-2378.

19. A. Tessmann, A. Leuther, C. Schwörer, H. Massler, W. Reinert, M. Walther, R. Lösch, and M. Schlechtweg, "Millimeter-Wave Circuits Based on Advanced Metamorphic HEMT Technology," *Proceedings IEEE 29th International Conference on Infrared and Millimeter Waves and 12th International Conference on Terahertz Electronics*, September 2004, pp. 165-166.

20. J. M. Rollin, G. I. Chance, and S. R. Davies, "A Membrane Planar Diode for 200 GHz Mixing Applications," *Proceedings IEEE 29th International Conference on Infrared and Millimeter Waves and 12th International Conference on Terahertz Electronics*, September 2004, pp. 205-206.

21. V. G. Bozhkov, "Semiconductor Detectors, Mixers and Frequency Multipliers for the Terahertz Band," *Radiophysics and Quantum Electronics*, **46**, 8-9, 2003, pp. 631-656.

22. V. S. Möttönen and A. V. Räisänen, "General Purpose Fifth-Harmonic Waveguide Mixer for 500-700 GHz," *Proc. 34th European Microwave Conference*, October 2004, pp. 1145-1147.

23. J. S. Rieh, B. Jagannathan, D. R. Greenberg, M. Meghelli, A. Rylyakov, F. Guarin, Z. Yang, D. C. Ahlgren, G. Freeman, P. Cottrell, and D. Harame, "SiGe Heterojunction Bipolar Transistors and Circuits Toward Terahertz Communication Applications," *IEEE Transactions on Microwave Theory and Techniques*, **MTT-52**, 10, October 2004, pp. 2390-2408.

24. V. Lubecke, K. Mizuno, and G. Rebeiz, "Micromachining for Terahertz Application," *IEEE Transactions on Microwave Theory and Techniques*, **MTT-46**, 11, November 1998, pp. 1821-1831.

25. H. Kazemi, S. T. Wooton, N. J. Cronin, S. R. Davies, R. E. Miles, R. D. Pollard, J. M. Chamberlain, D. P. Steenson, and J. W. Bowen, "Active Micromachined Integrated Terahertz Circuits," *International Journal of Infrared and Millimeter Waves*, **20**, 5, 1999, pp. 967-974.

26. S. Biber, J. Schür, and L.-P. Schmidt, "Technological Issues for Micromachining of New Passive THz-Components Based on Deep-Trench Silicon Etching," *Proceedings IEEE 29th International Conference on Infrared and Millimeter Waves and 12th International Conference on Terahertz Electronics*, September 2004, pp. 145-146.

27. A. Hirata, M. Harada, and T. Nagatsuma, "120-GHz Wireless Link Using Photonic Techniques for Generation, Modulation and Emission of Millimeter-Wave Signals," *IEEE Journal of Lightwave Technology*, **21**, 10, October 2003, pp. 2145-2153.

28. B. S. Meyerson, "IBM Microelectronics; Wireless Technology & Enablement," *World Wireless Research Forum (WWRF), Workshop in Paris*, December 6-7, 2001; available at http://www.wireless-world-research.org/meetings/WWRF4/doc/WWRF%20IBM%20Presentation.pdf.

29. A. J. Joseph, D. L. Harame, B. Jagannathan, D. Coolbaugh, D. Ahlgren, J. Magerlein, L. Lanzerotti, N. Feilchenfeld, S. St. Onge, J. Dunn, and E. Nowak, "Status and Direction of Communication Technologies – SiGe BiCMOS and RFCMOS," *Proc. IEEE*, **93**, 2005, pp. 1539-1558.

30. ITRS International Technology Roadmap for Semiconductors, 2004 Update, Overview and Summaries; available at http://www.itrs.net/ Links/2004Update/ 2004_00_Overview.pdf.

31. P. Asbeck, I. Galton, K. C. Wang, J. F. Jensen, A. K. Oki, and C. T. M. Chang, "Digital Signal Processing – Up to Microwave Frequencies," *IEEE Transactions on Microwave Theory and Techniques*, **MTT-50**, 3, March 2002, pp. 900-909.

32. E. Sano, "High-Speed Lightwave Communication ICs Based on III-V Compound Semiconductors," *IEEE Communications Magazine*, **39**, 1, January 2001, pp. 154-158.

33. M. P. M. Hall and L. W. Barclay, *Radiowave Propagation*, London, Peter Peregrinus Ltd., 1989.

34. R. K. Crane, "Fundamental Limitations Caused by RF Propagation," *Proceedings of the IEEE*, **69**, 2, February 1981, pp. 196-209.

35. B. Thomas, A. Maestrini, and G. Beaudin, "Design of a Broadband Sub-Harmonic Mixer Using Planar Schottky Diodes at 330 GHz," *Proceedings IEEE 29th International Conference on Infrared and Millimeter Waves and 12th International Conference on Terahertz Electronics*, September 2004, pp. 457-458.

36. "Guidelines for Limiting Exposure to Time-Varying Electric, Magnetic, and Electromagnetic Fields (Up to 300 GHz)," ICNIRP Guidelines.

37. P. F. Driessen, "Gigabit/s Indoor Wireless Systems with Directional Antennas," *IEEE Transactions on Communications*, **44**, 8, August 1996, pp. 1034-1043.

38. R. Piesiewicz, T. Kleine-Ostmann, N. Krumbholz, D. Mittleman, M. Koch, and T. Kürner, "Terahertz Characterisation of Building Materials," *Electronics Letters*, **41**, 18, September 2005, pp. 1002-1004.

39. D. Turchinovich, A. Kammoun, P. Knobloch, T. Dobbertin, and M. Koch, "Flexible All-Plastic Mirrors for the THz Range," *Applied Physics A*, **74**, 2002, pp. 291-293.

40. P. Knobloch, D. Turchinovich, T. Dobbertin, and M. Koch, *Optical Component*, US patent 6,954,309 B2, October 11, 2005.

41. R. Piesiewicz, K. Baaske, K. Gerlach, M. Koch, and T. Kürner, "The Potential of Dielectric Mirrors as Key Elements in Future Non-Line-of-Sight Indoor Terahertz Communication Systems," *Proc. 16th Intl. Symp. on Space Terahertz Technology*, Göteborg, Sweden, May 2005.

42. N. Krumbholz, K. Gerlach, F. Rutz, M. Koch, R. Piesiewicz, T. Kürner, and D. Mittleman, "Omnidirectional Terahertz Mirrors: A Key Element for Future Terahertz Communication Systems," *Applied Physics Letters*, **88**, 2006, 202905.

43. J. D. Kraus and R. J. Marhefka, *Antennas for All Applications*, New York, McGraw Hill, 2002.

44. W. L. Stutzman and G. A. Thiele, *Antenna Theory and Design*, New York, John Wiley & Sons, 1981.

45. C. A. Balanis, *Antenna Theory, Analysis and Design*, New York, John Wiley & Sons, 1982.

46. T. K. Sarkar, Z. Ji, K. Kim, A. Medouri, and M. Salazar-Palma, "A Survey of Various Propagation Models for Mobile Communication," *IEEE Antennas and Propagation Magazine*, **45**, 3, June 2003, pp. 51-82.

47. R. Vaughan and J. B. Andersen, *Channels, Propagation and Antennas for Mobile Communications*, London, IEE Press, 2003.

Introducing the Feature Article Authors

Radoslaw Piesiewicz was born in Koszalin, Poland, in 1976. He received the International Baccalaureate Bilingual Diploma IB, issued in Geneva, Switzerland, in 1996. He then studied economics at the Warsaw School of Economics from 1996 to 1997. Afterwards, he studied electrical engineering at the Technical University of Gdansk (Poland) from 1997 to 2002, where he earned a MSEE degree in Microwave Engineering with highest honors. From 2002 to 2004, he was with Fraunhofer Institut IZM, Advanced Systems Engineering in Paderborn, Germany, where he worked on electromagnetic compatibility problems in multilayer circuits in the framework of the EU Project MESDIE. From 2004 until now, he has been a project research engineer working towards the PhD degree at the Institut für Nachrichtentechnik at the Technical University of Braunschweig and in the Terahertz Communications Lab in Braunschweig. His working areas are PHY-layer aspects of ultra-broadband multi-gigabit wireless communication systems at frequencies above 60 GHz. The focus is on the system modeling, simulation, and design, as well as on the propagation aspects in bound and unbound media, including measurements and modeling. He is an active expert evaluator in the field of communication systems for the European Commission in Brussels.

Thomas Kleine-Ostmann was born in Lemgo, Germany, in 1975. He studied electrical engineering at Virginia Polytechnic Institute and State University, USA (specializing in communications), where he received the MSc degree in 1999. He studied at the Technical University Braunschweig (specializing in radio-frequency engineering), where he received the Dipl.-Ing. degree in 2001. In 2005, he received the Dr.-Ing. degree, also from Technical University Braunschweig.

He worked as a research assistant in the Ultrafast Optics Group at JILA in Boulder, Colorado, USA, and in the Semiconductor Group at Physikalisch-Technische Bundesanstalt, in Braunschweig, Germany, before he started working on his PhD in the field of THz spectroscopy at the Institut für Hochfrequenztechnik at Technical University Braunschweig. Since 2006, he has been working as a permanent scientist in the Electromagnetic Fields Group at Physikalisch-Technische Bundesanstalt in Braunschweig, Germany. He is currently working on realization and transfer of electromagnetic field strength, electromagnetic compatibility, and on THz metrology.

Dr. Kleine-Ostmann is a member of the German Association of Electrical Engineers (VDE). He received the Kaiser-Friedrich research award for his work on a continuous-wave THz imaging system in 2003.

Norman Krumbholz was born on August 30, 1979, in Wolfsburg, Germany. From 2000 to 2005, he studied the joint program of business administration and electrical engineering at the Technical University of Braunschweig, Germany. He performed research for his master's thesis at Rice University in Houston, TX. He is currently working towards his PhD degree in Electrical Engineering at the Institute for High-Frequency Technology at the Technical University of Braunschweig. Fiber-coupled THz spectroscopy systems for use in an industrial environment and THz communications are his main research areas.

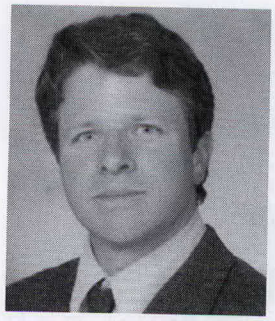

Daniel Mittleman received his BS in Physics from the Massachusetts Institute of Technology in 1988. He then went on to the University of California, Berkeley, where he joined the research group of Dr. Charles Shank. His primary research involved the spectroscopy of semiconductor nanocrystals using laser pulses with durations of less than 20 femtoseconds, at wavelengths from 480 nm to 670 nm. These experiments were performed in collaboration with the Alivisatos group in the Chemistry Department at Berkeley, and were carried out at the Lawrence Berkeley National Laboratory. Dr. Mittleman received his MS in 1990, and his PhD in 1994, both in Physics.

Dr. Mittleman then joined the research group of Dr. Richard Freeman as a Postdoctoral Member of the Technical Staff at AT&T Bell Laboratories. While there, he pursued research into high-harmonic generation in noble gases using a 100 femtosecond, one-terawatt laser system. When Dr. Freeman left Bell Labs in early 1995, Dr. Mittleman began working with Dr. Martin Nuss, who, with his previous post-doc Dr. Binbin Hu, had recently pioneered the use of THz time-domain spectroscopy for imaging. Dr. Mittleman's work in this laboratory included the non-contact characterization of doped semiconductor wafers using the THz Hall effect, the construction of a THz imaging system in a reflection geometry for use in "T-ray tomography" measurements, and the THz spectroscopy of inverse micelles of water in heptane. During this time, AT&T split into three companies, and most of Bell Labs became part of one of the three pieces, Lucent Technologies. Dr. Mittleman joined the ECE Department at Rice University in September 1996. He is affiliated with the Rice Quantum Institute.

Martin Koch was born in Marburg, Germany, in 1963. He received the Diploma and PhD degrees in Physics from the University of Marburg in 1991 and 1995, respectively. From 1995 to 1996, he was a post-doc at Bell Labs/Lucent Technologies, Holmdel, NJ. From 1996 to 1998, he worked in the photonics and optoelectronics group at the University of Munich. Since 1998, he has been an Associate Professor at the Technical University of Braunschweig in the Electrical Engineering Department. In 2003, he did a three-month sabbatical at the University of California in Santa Barbara. He was also awarded the Kaiser-Friedrich Research Price in 2003.

Joerg Schoebel received the Diploma and PhD in Electrical Engineering from the Technical University (TU) of Braunschweig, Germany, in 1994 and 2000, respectively.

In 1994, he worked for Hewlett-Packard in Boeblingen, Germany, on external-cavity tunable laser sources. During 1995, he was a visiting scientist at AT&T Bell Labs, Holmdel, NJ, where he was involved in the assessment of silicon oxidation technologies for flash memory. He joined the Department of RF Engineering of the TU Braunschweig as a research scientist in 1996, where he focused on organic light-emitting diodes (OLEDs). He investigated energy-level structures and charge-injection properties of organic hetero-interfaces and contacts in OLEDs with photoelectron spectroscopy and (thermo-)electrical techniques. From 2001 to 2005, he was employed with Robert Bosch corporate research and advanced engineering. He was involved in research on automotive radar systems with phased-array antennas, digital-beamforming radar, array signal processing, and in the integration of automotive-compliant radar demonstrators. He further led the Bosch activities on RF MEMS (micro-electromechanical systems for RF applications) and coordinated several work packages in the EC-funded research project "MIPA." In this project, RF-MEMS technology was applied to beam-steering antenna front ends for automotive radar at 77 GHz. His contributions addressed all aspects of the antenna front end: from system and antenna design to RF-MEMS switches and components, and also packaging and interconnect technology. Since December, 2005, he has been a Professor for microwave engineering at the TU Braunschweig, Germany. His research interests include systems and components for sub-millimeter-wavelength communications; automotive radar and motion sensors, in particular the design of RF and antenna front ends; RF MEMS; planar RF circuit and antenna technology; array antennas; beam forming and array signal processing; and electronic bandgap structures and metamaterials. Prof. Schoebel has coauthored more than 40 scientific publications and had 17 patent applications.

Thomas Kürner, was born in Tailfingen, Germany, in 1964. He received the Dipl.-Ing. degree in Electrical Engineering from the University of Karlsruhe, Germany, in 1990, and the Dr.-Ing. degree in 1993 from the same university. From 1990 to 1994, he was with the Institut für Höchstfrequenztechnik und Elektronik (IHE) at the University of Karlsruhe, working on wave-propagation

modeling, radio-channel characterization, and radio-network planning. Until 1994, he was also a lecturer for the Carl Cranz Series for scientific education, teaching wave-propagation modeling and channel characterization. From 1994 to 2003, he was with the radio network planning department at the headquarters of the GSM 1800 and UMTS operator E-Plus Mobilfunk GmbH & Co. KG, Düsseldorf. There he was the team manager for radio network planning support, responsible for radio network planning tools, propagation models, algorithms, processes, and parameters. Since 2003, he has been a Professor for Mobile Radio Systems at the Institut für Nachrichtentechnik at the Technical University of Braunschweig. His working areas are propagation, traffic and mobility models for automatic planning of mobile radio networks, planning of hybrid networks, car-to-X-communication, as well as indoor channel characterization for high-speed short-range systems including future terahertz communication systems. He has been engaged in several international bodies, such as ITU-R SG 3 (radio wave propagation), UMTS Forum Spectrum Aspects Group, COST 231, COST 273, COST 2100, and COST 259, where he chaired the working group "Network Aspects." He was also a work-package leader in the European IST-MOMENTUM project, working on methods for "Automatic Planning of Large-Scale Radio Networks." He was Vice Chair of the 2007 European Conference on Antennas and Propagation. Prof. Kürner received the "ITG-Förderpreis" Award from the German VDE for his PhD thesis in 1994, and in 1995 he was awarded the IEE/ICAP'93 Best Propagation Paper Award.